



Comparative Analysis of Improved Aerodynamic Performance: Computational Fluid Dynamics Study of the Trailing Edge Morphing Concept Parameters

Arafat Kabir¹ · Abdulkareem Sh. Mahdi Al-Obaidi¹ · Felicia Wong Yen Myan¹

Received: 27 December 2023 / Revised: 16 March 2024 / Accepted: 10 May 2024
© The Author(s), under exclusive licence to The Korean Society for Aeronautical & Space Sciences 2024

Abstract

The trailing edge morphing concept in aircraft wings has been utilized and implemented for a long time. Airfoil aerodynamic investigation can be made to identify the optimal wing configuration for trailing edge morphing providing enhanced performance but lacks sophisticated methods to identify and quantify these optimal wing configurations which shows a significant challenge in aircraft wing engineering. In this paper, the aerodynamic performance of trailing edge morphing wing configurations is investigated to determine the most effective wing configurations based on flight phases. Various wing configurations created by the trailing edge morphing concept could bring aerodynamic advantages and disadvantages, hence the aerodynamics understanding, and results remain unknown. Based on the flight conditions, the requirements for optimal aerodynamic performance are different, which can be fulfilled by optimal configurations based on the morphing concept applied. Variable trailing edge morphing concept used individually to run extensive performance analysis for obtaining optimal morphing wing configurations. By changing the bending angle and bending location, morphing concepts are applied to symmetric and asymmetric airfoils to generate 100 unique morphing wing configurations by changing the geometry coordinates using X-foil and Javafoil. To support the sophisticated analysis, computational fluid dynamics testing was conducted at 303,100 Reynolds numbers at subsonic speeds using ANSYS to evaluate lift and drag performance. Based on aerodynamic data, the optimal wing configurations providing optimal aerodynamic performance for specific flight phases were highlighted. Drag reduction and lift improvement efficiency at various ranges were identified and evaluated to identify optimal wing configurations for cruise, take off and climbing flight phases.

Keywords Aerodynamics · Airfoil · CFD · Trailing edge morphing · Lift coefficient & drag coefficient

1 Introduction

The observation of birds flying inspired flight and aerodynamics. Humans developed aircraft from that idea. Traditional aircraft wings have a fixed wing configuration, while

birds can change their wing shape to achieve variable wing configurations [1]. The bird typically changes its wing shape by twisting, folding, and other transformation to manipulate the aerodynamic performance and stability to its optimal level [2, 3]. Morphing technology in aircraft wings attempts to match the aerodynamic performance of conventional wings, but current technology limits wing shape transformation [4–6]. Therefore, the main aspect of morphing wings is to obtain variable wing configurations in the conventional wing. Big aerodynamic research centers like NASA MIT, currently working endlessly to obtain as many optimal wing configurations as possible using morphing technologies [7].

The morphing concept can be applied in both conventional and non-conventional wings. Achieving optimal aerodynamic performance from these wing configurations requires a lot of aerodynamic investigation and experiments [4].

Communicated by Eunji Jun.

✉ Arafat Kabir
kabirarafat@hotmail.com

Abdulkareem Sh. Mahdi Al-Obaidi
abdulkareem.mahdi@taylors.edu.my

Felicia Wong Yen Myan
feliciayenmyan.wong@taylors.edu.my

¹ School of Computer Science and Engineering, Taylor's University, No. 1 Jalan Taylor's, 47500 Subang Jaya, Selangor Darul Ehsan, Malaysia

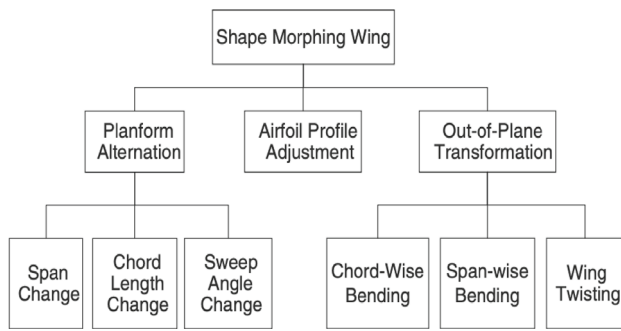


Fig. 1 Morphing categories [5]

Morphing technology can be used in conventional and unconventional aerodynamic air vehicle wings, drones, missiles, UAVs, spacecraft, and more [5, 6]. Figure 1 shows three types of morphing wings that identify and design all these morphing concepts. Airfoil configuration changes are different and correlated between these categories. To optimize performance, each wing morphing type changes the wing configuration differently. Planform alternation, out-of-plane transformation, and airfoil profile adjustment (airfoil-level morphing) are morphing wings.

Now, that morphing concepts can create different wing configurations, finding the best one for performance is the hardest part. Thus, aerodynamic research is needed to test and discover morphing wing configurations that are generated and modified for maximum performance before a conventional wing with morphing technology can be built. Airfoil aerodynamic analysis is the foundational study. Aerodynamic research on a full-scale or high-scale morphing wing can be expensive and time-consuming. Since morphing technology allows many wing configurations, it would be difficult to find the best one for performance. Finding the best morphing concept for specific flight phases may be difficult. This research could benefit aerodynamicists by providing a deeper understanding of the morphing concept and helping the aircraft industry develop innovative conventional morphing wings.

Morphing airfoils improve aerodynamics and fuel efficiency. Morphing wings perform better because they can change shape and geometry. For different flight phases, optimal aerodynamic performance and wing configurations vary. The optimal morphing wing configuration must be determined from morphing technology's variation to design the right one. Thus, evaluating the aerodynamic performance of wing configurations with morphing concepts will help identify the best morphing concepts for an airfoil with optimal aerodynamic performance and stability.

Aerodynamic analysis is needed before designing a conventional wing with morphing concepts. Theory, computational fluid dynamics (CFD), and wind tunnel testing

determine lift and drag in aerodynamic analysis. Aerodynamic analysis can range from low-speed airfoil testing to supersonic analysis. Low-speed airfoil wing testing is the first step in this study for each airfoil configuration. The analysis obtains Lift and drag coefficients (C_L) (C_D) at various angles of attack (AOA) and Reynolds numbers, leading to the optimal morphing wing configuration. Morphing technology optimized aircraft performance and stability. An aerodynamic analysis is needed before designing a conventional wing with morphing concepts. Theory, CFD, and wind tunnel testing determine lift and drag in aerodynamic analysis. Aerodynamic analysis can range from low-speed airfoil testing to supersonic analysis. Low-speed airfoil wing testing is the first step in this study for each airfoil configuration [8–10]. The focus of this research is to evaluate and investigate the key morphing concepts of a low-speed airfoil and design of airfoils with optimal morphing wing configuration. This avoids having to construct a full-scale wing and conduct extensive aerodynamic analysis for every airfoil wing configuration formed by morphing a wing [11]. Based on the primary investigation, optimal wing configurations can be implemented in a full-scale morphing wing and extensively analyzed to determine aerodynamic efficiency. A 3D wing will form from the morphing shape after the final transformation. From the morphing wing's wing configurations, the optimal one can be determined using CFD and wind tunnel testing [8, 11, 12]. It will also help to determine the correct method or approach to using a morphing wing designed to implement the morphing concept. After optimal morphing concepts are identified, multiple optimal configurations will be implemented to understand and verify their integrated performance. This study is limited to the analysis of C_L and C_D to identify and build the optimal morphing wing configurations.

This research will determine the best morphing wing configuration for aerodynamic efficiency. It will also determine the best way to use a morphing wing to implement the concepts individually and in a wing configuration. This design can achieve any wing configuration for better aerodynamic performance in any flight condition or phase. Aerodynamic results can be used to analyze fuel efficiency, simulation, range, duration, endurance, and aircraft envelope. Design fuel-efficient civil and commercial airplanes by implanting optimal wing configurations in conventional wings. An optimal morphing wing configuration will improve aircraft performance and reduce fuel consumption and pollution. This foundational study may help aerodynamicists understand the morphing principle and help the aviation industry develop unique conventional morphing wings.

2 AIRFOIL Morphing Based on the Variable Trailing Edge

An experimental analysis was made for a morphing structure where trailing edges of the airfoil Wortmann FX63-137, as shown in Fig. 2 [13]. The morphing structure deformed with the help of an actuator to change the position of the trailing edge. The deflection causes the morphing structure to deform downward at an angle known as the morphing angle or flap angle.

The structure was deformed, and the morphing angle varied from a stationary position of -30° to 40° . The wind tunnel testing was conducted to determine the coefficient of lift at various morphing angles and the angle of attack was also varied as well. At Reynolds, no 1×10^6 , the coefficient of lift is increased as shown in Fig. 3. At the lower angle of attack, the lift coefficient is lower than the reference value for the morphing angle below 10° . As the morphing angle increases at a lower angle of attack, the lift coefficient increases significantly. For example, at 0 angles of attack, about 26° of morphing angle the lift coefficient is 1 while in the unmorphed or the regular wing, the lift coefficient is 0.75. The lift coefficient increased by 25%, which is a significant improvement in aerodynamic performance. It shows similar behavior for the angle of attack from 0° to 15° . After an AOA of 10° , the change of lift coefficient reduces as the morphing angle varies. At the angle of attack of 20° , the lift coefficient of the morphing airfoil remains the same as the regular wing.

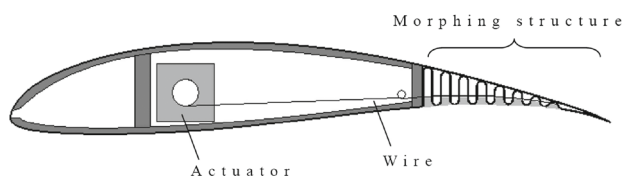


Fig. 2 Implementation of the morphing structure of FX63-137 [13]

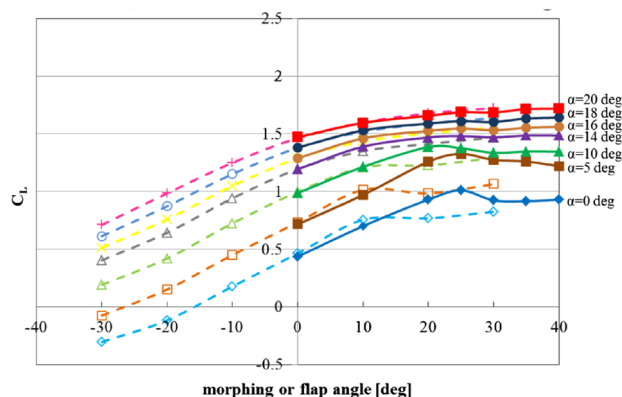


Fig. 3 Results of the wind-tunnel experiment of morphed FX63-137 at $Re = 1 \times 10^6$ [13]

In terms of variable camber trailing edge, the morphing or flap angle did not show significant improvement at a higher angle of attack of more than 15° . But for the lower angle of attack, below 15° , it shows improvement in higher morphing or flap angle ranging from 10° to 30° flap angle. Table 1 shows the ranges and estimate of C_L improvements, obtained from the result in Fig. 3.

In another experiment, the trailing edge position of the airfoil NACA 0012 varied using a morphing flap, where the aerodynamic performance of the airfoil with a morphing flap was compared with the wings with a conventional flap using CFD simulation [14]. The objective of this investigation was to determine the improvement of aerodynamic performance and stability. For wings with conventional flaps, the flap length C_f remains fixed. In terms of the morphing flap, the flap length can be varied as shown in Fig. 4. The use of flap is traditionally used to increase lift force during take-off and increase drag during landing.

The experiment carried out a CFD simulation of a morphing flap at variable length and compared it with a flap with fixed flap length C_f the CFD simulation was run at variable Mach no ranging from 0.4 to 0.875. The morphing flap showed an increase in aerodynamic force and moment compared to the fixed flap. This means a wing with a morphing flap will require a shorter distance and time for take-off and landing, leading to a reduction in fuel consumption and shorter time. In terms of flutter frequency and velocity, it demonstrated more controlled behavior compared to conventional flaps showing more stability. Having more controlled flutter frequency and speed minimizes the risk of damaging flaps and wing structure due to vibration and flutter produced during flight [15–17].

The trailing edge showed significant improvement, after reviewing multiple studies it is clear, at lower angles of attack there is a significant change in the increase of lift coefficient and decrease in drag coefficient, resulting in lift-to-drag ratio change. The range of trailing edge bending angle, or morphing angle is yet to be identified for a symmetric airfoil and an asymmetric airfoil. Another parameter that can be varied is the morphing flap length. This will identify the optimal flap length and gives optimal aerodynamic performance for a fixed chord length.

In another study, the trailing edge concept was implemented at a fixed bending location in asymmetric airfoil NACA 23012 to improve C_L and C_D . According to Fig. 5, the morphing location for trailing edge bending took place at 85% of the chord location and the bending took place from -4° to 8° . NMCC 2 configuration according to Fig. 5, shows anticlockwise trailing edge bending at -4° and MCC4 shows 8° clockwise bending.

CFD simulation was conducted for this experiment to measure aerodynamic coefficient for the trailing edge bending in 2D airfoil. According to Fig. 6 C_l results were plotted

based on the trailing edge bending for NACA 23012. Based on the results, it is clear that the NMCC 2 airfoil, trailing edge bending at -4° shows the lowest C_L and MCC4 airfoil, trailing edge bending at 8° showed highest C_L . But the bending range for this study is quite low. But for AOA above 12-degree variation occurs. According to Fig. 7, the C_D results represented based on the AOA for airfoil configurations based on the variable morphing concept. The drag for the higher clockwise bending appears to be higher and followed for anti-clockwise trailing edge bending the drag appears to be lower. This evaluation is more significant when the AOA is above 5° , still few variations can be found.

Wing flap was evaluated in one study based on flap designs. Figure 8, shows three airfoils, where the baseline airfoil is the regular S809 airfoil, the conventional flap showing the same airfoil with trailing edge bending of -10° at 70% chord location and morphing flap is the similar like the conventional flap but the flap has a wave like design in trailing edge. That means within the flaps there is a modification which can be seen S809 morphing flap airfoil. But aerodynamic performance analysis based on the study showed that conventional flap which consist of just trailing edge morphing showed better optimal performance compared to morphing flap in terms of C_L , C_D and C_L/C_D [19].

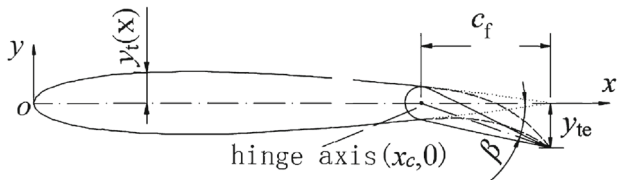


Fig. 4 Schematics and measurement of a conventional flap with flap length [14]

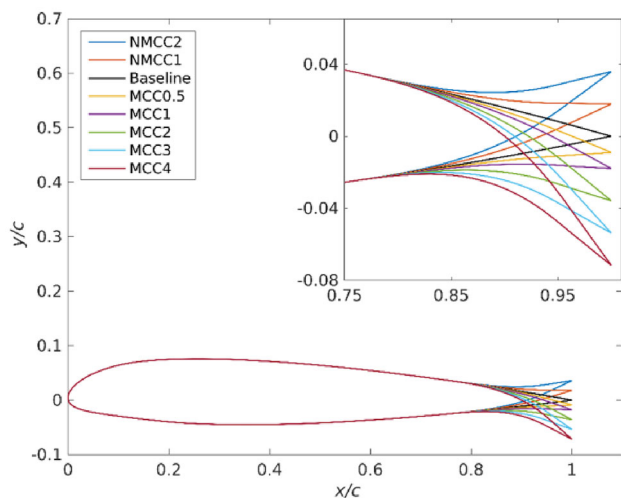


Fig. 5 Outline of Trailing edge bending of NACA 23012 [18]

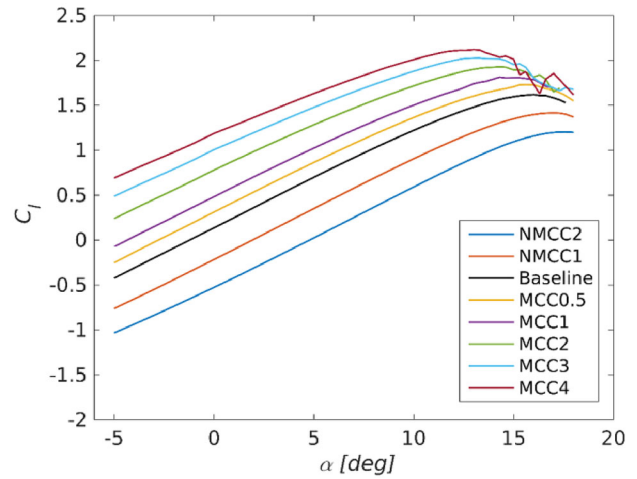


Fig. 6 C_L result of trailing edge morphing wings from -4 degree till 8 degree bending angle [18]

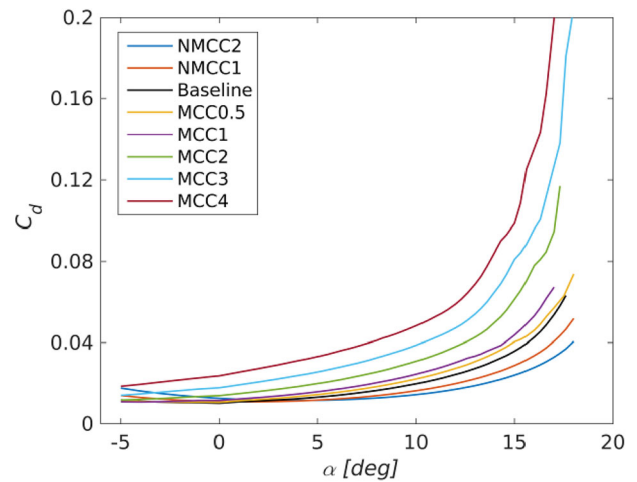


Fig. 7 C_D result of trailing edge morphing wings from -4 degree till 8 degree bending angle [18]

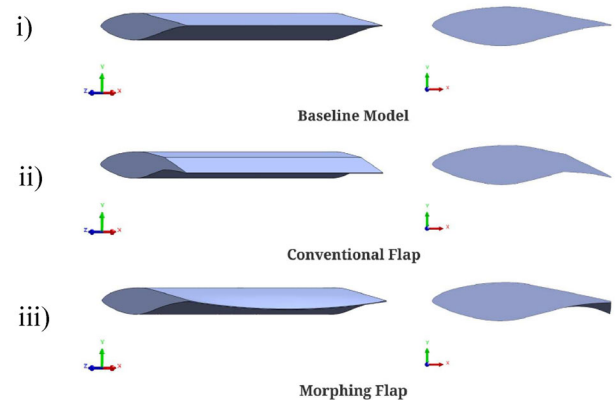


Fig. 8 (i) Wing design of S809 airfoil, (ii) Conventional flap with trailing edge morphing in S809 airfoil and (iii) Trailing edge bending of S809 with morphing design on trailing edge [19]

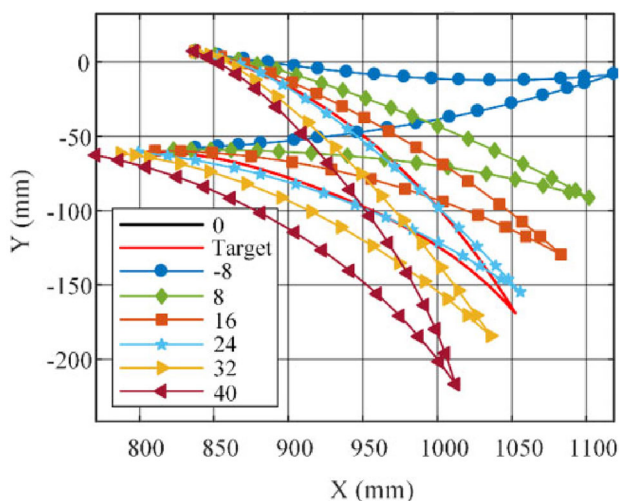
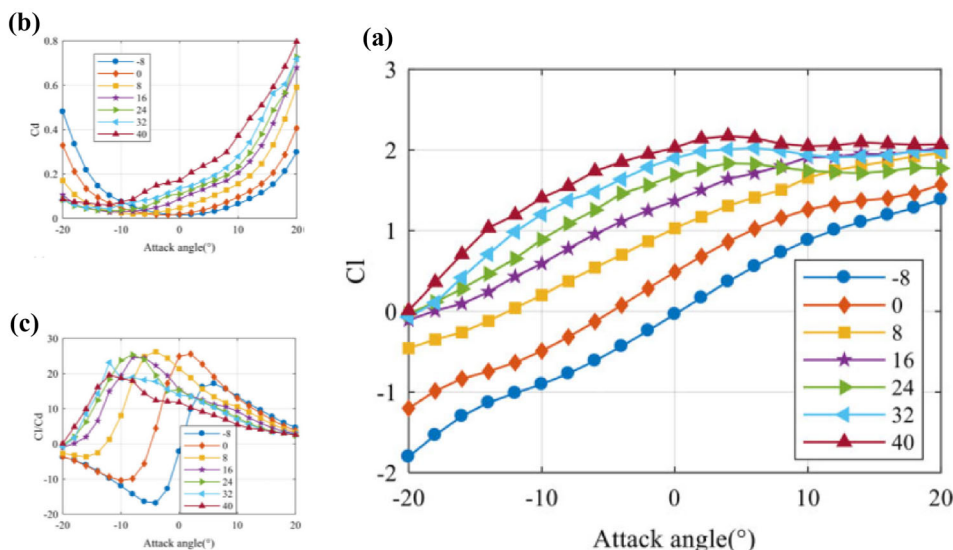


Fig. 9 Trailing edge morphing parameters of bending ranging from -8° till 40° [20]

Trailing edge morphing was implemented in a NACA 2412 airfoil in a study and aerodynamic analysis was conducted using CFD ANSYS software, where C_L and C_D were evaluated [20]. Figure 9 shows the trailing edge bending took place at a fixed bending location and bending angle ranging from -8° to 40° . According to Fig. 10, C_L increases as the bending angle increases for the AOA up to 10° ; for C_D , there is variation as the trailing edge bending takes place; both coefficients vary at different AOA; and for C_L/C_D improvements found when the trailing edge bending ranges from -8° to 8° . The bending range needs to be evaluated in different or similar airfoil to narrow down specific wing configurations that will show optimal aerodynamic performance according to flight phases.

Fig. 10 Aerodynamic analysis of trailing edge morphing based on bending angle, **a** C_L against AOA, **b** C_D against AOA and **c** C_L/C_D against AOA [20]



Although these studies introduced and showed aerodynamic results based on small ranges of trailing edge bending angle and fixed morphing location, there are still significant gaps found in the reviewed studies. Overall research gaps identified based on the reviewed studies:

- Ranges of trailing edge bending angle for both clockwise and anti-clockwise are limited.
- Trailing edge bending locations in the reviewed studies are fixed, bending location is a significant parameter to be evaluated for optimal aerodynamic performance.
- Aerodynamic coefficient graphs shown, where variations and minor significant aerodynamic relations are found in respect to morphing parameters.
- No tabulated data included where percentage difference of each trailing edge morphing airfoil configuration can be evaluated for significant aerodynamic improvement for specific flight phases.

The trailing edge showed significant improvement, after reviewing multiple studies its clear, at lower AOA there is a significant change in the increase of C_L and decrease in C_D , resulting in C_L/C_D change. The range of trailing edge bending angle, or morphing angle is yet to be identified for a symmetric airfoil and an asymmetric airfoil. Another parameter that can be varied is the morphing flap length. This will identify the optimal flap length and gives optimal aerodynamic performance for a fixed chord length.

3 Understanding and Measuring Aerodynamic Performance

The root of measuring the aerodynamic performance and efficiency is lift and drag coefficients, these variables are part of

lift and drag forces induced respectively. This simple assessment is based on the performance of a wing. Equations (1) and (2) represents the lift and drag forces of a wing at a given flight condition:

$$L = \frac{C_L \rho V^2 A}{2}, \quad (1)$$

$$D = \frac{C_D \rho V^2 A}{2}. \quad (2)$$

Based on the Lift and drag force equation, lift, and drag coefficients can be deduced as shown in Eqs. (3) and (4) respectively:

$$C_L = \frac{2L}{\rho V^2 A}, \quad (3)$$

$$C_D = \frac{2D}{\rho V^2 A}. \quad (4)$$

Based on the flight phases the impact of lift and drag coefficient varied, Table 2 shows the equations of important aerodynamic measures and their relationship with the coefficients.

To achieve optimal level flight performance, the generated forces or force coefficients can be used to determine lift and drag increments. Table 3 shows where to increase or decrease lift and drag for optimal performance at each significant flight phase and how this affects flight performance and economic value.

Tables 2 and 3 show the C_L and C_D requirements for flight phases for optimal performance. The C_L and C_D result differences between the reference airfoils will be evaluated after designing all the morphing airfoils based on individual concepts. The percentage difference will be tabulated and sets of aerodynamic results will be plotted in a graph. Table 4 shows methods to evaluate the simulated lift and drag-coefficient results compared with the reference value to identify optimal configuration and performance according to each flight-phase requirement.

The initial step is to Choose a symmetric airfoil and an asymmetric airfoil. Reference airfoils will have a chord length of 1 m and a span of 1 m. The CFD simulation will be similar to wind tunnel testing, where ANSYS software is used to generate C_L and C_D of the airfoils within the stall angle range [8, 10–12]. A conventional wing has a higher wing area meaning the experimental airfoils are scaled down to a smaller size using similarity rules [21, 22]. Aerodynamic results obtained from the designed and morphing airfoils will be compared with the reference airfoil chosen initially. The percentage difference between the lift and drag-coefficient results will help identify the optimal configuration suitable for the flight phases. The results will be evaluated on

the significant difference between lift coefficient results and drag-coefficient results and based on the requirements for the flight phases mentioned in Tables 2 and 3. The percentage difference of any variables is calculated based on Eq. (10) and percentage error based on Eq. (11).

$$\begin{aligned} \text{Percentage difference} \\ &= \frac{\text{morphing variable} - \text{reference variable}}{\text{reference variable}} \times 100, \quad (10) \end{aligned}$$

$$\begin{aligned} \text{Percentage error} \\ &= \frac{\text{Generated variable} - \text{theoretical variable}}{\text{theoretical variable}} \times 100. \quad (11) \end{aligned}$$

4 Designs of Morphing NACA 0012 and NACA 2415 and Reference Validation

ANSYS CFD simulation was conducted on both symmetric airfoil NACA 0012 and asymmetric airfoil NACA 2415. The results of the C_L will be compared to verify the designed reference airfoils for CFD. The Reynolds number will be set at 303,100, which is the same reference as NACA 2415 reference airfoil data, and studies have shown that CFD analysis at this Reynolds number range generated accurate aerodynamic results for subsonic speeds [11, 12, 23]. The appropriate fluent turbulent model was identified, and grid independent meshing test (GIT) analysis was conducted, before the validation of the reference airfoils to ensure accurate aerodynamic results with percentage error less than 10%. After validation, the designed morphing airfoils undergo CFD simulation generating aerodynamic results under a similar setup. This process was also applied to other morphing concepts, such as variable scale and variable span; overall, each stage was taken to ensure the CFD fluid simulation generated accurate data [24].

4.1 Design of Airfoils with Trailing Edge Morphing Configuration

Based on the morphing concepts chosen, the airfoil configurations of NACA 0012 and 2415 were modified by changing the airfoil geometry coordinates, respectively. The design will be verified by CFD simulation at an AOA. Prior to the simulation, successful meshing and a fluent setup for the new design were ensured.

Airfoil configurations consist of a variable trailing edge obtained using an x-foil. Coordinates of each set of configurations of an airfoil at the morphing or bending angle of the trailing edge, ranging from -45° to 45° . The coordinates of each set of airfoil configurations will be obtained for every 10-degree morphing angle. Each set of coordinates

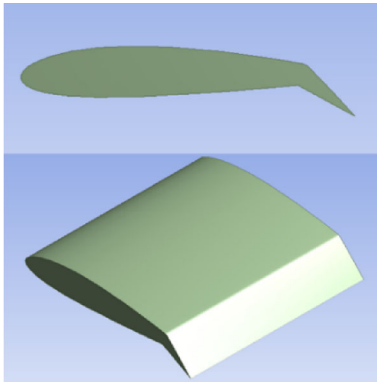


Fig. 11 NACA 2415 morphing length at 80% of chord for 35°

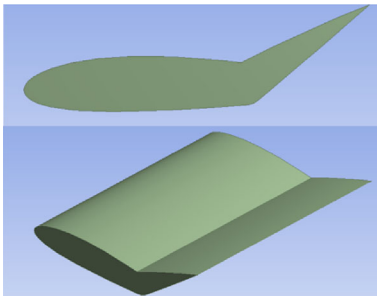


Fig. 12 NACA 2415 morphing length at 60% of chord for -35°

obtained will be used to design a 3D wing for each configuration of the trailing edge. The same method used for CFD simulation, except the input geometry will be the coordinates obtained for each airfoil set of variable trailing edges. This method will be repeated when the morphing flap length is varied to obtain new sets of wing configurations based on the morphing flap length. keynotes and parameters considered for designing trailing edge morphing airfoils for the research include:

- The morphing flap length varied from 90%, 80%, 70%, 60%, and 50% of the chord length. Figures 11 and 12 show morphing trailing edge bending at two different locations.
- The morphing bending angle ranged from -45° to 45°, at each morphing length. Figures 11 and 12 show morphing trailing edge airfoil at two different bending angles.
- There are 100 total wing configurations, 50 symmetric and 50 asymmetric.

4.2 Validation of NACA 0012 and 2415

After GIT was done, CFD simulations were run on symmetric and asymmetric airfoils at different AOA. Table 5 compares the NACA 2415 CFD simulation C_L result to reference data and is also plotted in a graph in Fig. 13. Figure 14 exhibits

a comparison between the NACA 0012 graph and the reference data graph. Based on the analysis, the reference airfoils were validated with a percentage error of less than 10%. Then, the set of aerodynamic data on C_L and C_D derived from CFD analysis, which is called reference data and will be compared to the morphing airfoils, will be presented. Following the validation of reference data for both symmetrical and asymmetrical airfoils, a new set of reference data was developed using CFD for a new set of attack angles ranging from -10° to 15°; this new set of attack angles will also be comparable to the morphing wing configurations. The new reference data for NACA 2415 and NACA 0012 based on the new AOAs are shown in Tables 6 and 7.

4.3 CFD Limitation

The C_D is expected to be higher due to the induced drag produced by finite wing spans [25]. Post fluent verification, the reference data considered includes the C_D generated from the reference airfoils. The AOA range for each designed morphing airfoil will be within the stall angle. CFD simulation will be similar to wind tunnel testing and ANSYS is a CFD tool used to generate C_L and C_D results and evaluate the percentages of difference with reference airfoils [24]. 3D wing in CFD simulation provides more realistic and accurate results compared to the 2D airfoil. CFD simulation of a 2D airfoil provides limited results and could not cover some aspects of 3D finite wing or wing-like trailing vortices and also when simulation undergoes turbulent flow [26, 27]. The reference airfoils scaled down to a chord length of 1 m, based on basic similarity rule and Reynolds number can be higher considering the speed of the inlet velocity is under the subsonic speed limit [21, 22].

5 Morphing Trailing Edge Airfoil CFD Results

The C_L and C_D results were reviewed to identify aerodynamic efficiency. The generated data from the designed airfoils showed better C_L and C_L/C_D than the reference data. Based on the comparison, the aerodynamic performance of an optimal airfoil wing configuration was identified. Optimal morphing configurations based on individual morphing concepts are identified, and both concepts are combined to obtain a hybrid airfoil optimal for a flight phase. The hybrid morphing airfoils undergo wind tunnel testing for further investigation to understand the implication of multiple optimal concepts in an airfoil. The aerodynamic results were compared in the same way with the reference airfoil and showed improved performance.

Fig. 13 C_L result of fluent verification NACA 2415 at Reynolds number 303100

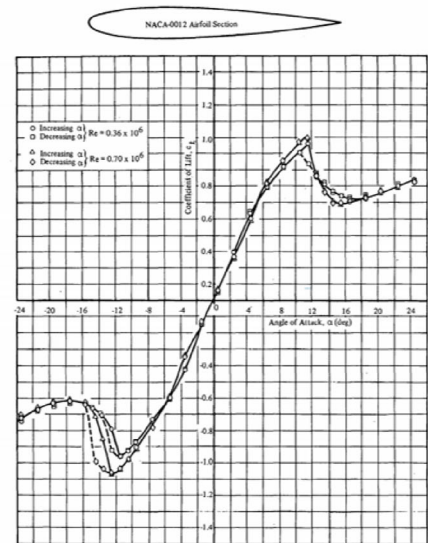
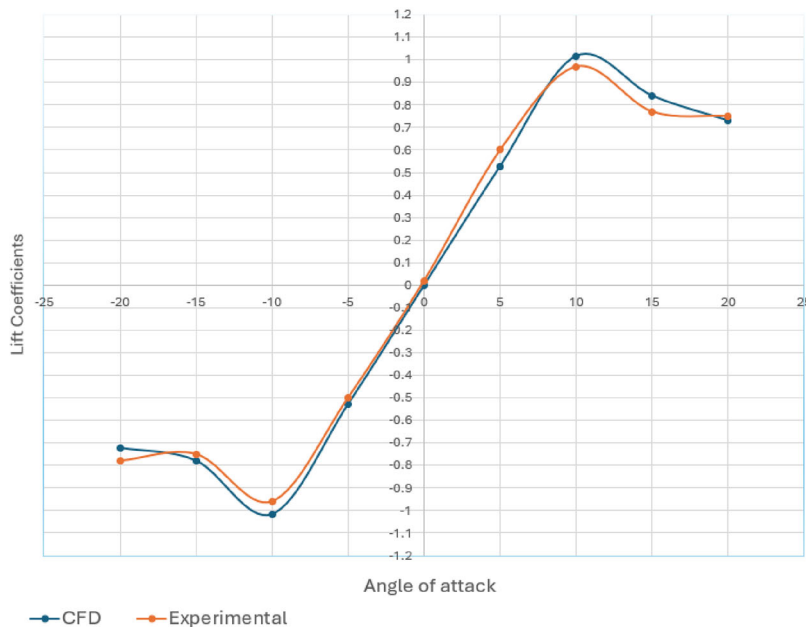
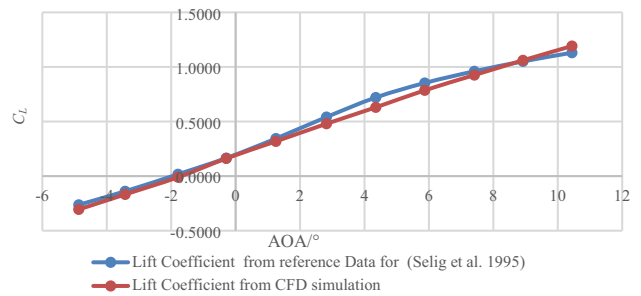


Figure 4 Section Lift Coefficients for the NACA-0012 Airfoil at Reynolds Numbers of 0.36×10^6 and 0.70×10^6

Fig. 14 C_L result of fluent verification NACA 0012 at $Re = 303,100$ compared with reference data

5.1 Trailing Edge Morphing for Asymmetric Airfoil NACA 2415

The CFD analysis established some distinguished findings for trailing morphing for NACA 2415. This helped narrow down the significant design points or wing configurations preferred for the specific flight phases. Table 4 was used to fulfill the requirement of C_L and C_D results and to find the design points preferred for the flight phases. But initially, it started with an individual assessment of each morphing distance or bending distance based on chord location. The CFD results were evaluated individually for each location to determine the effect of the bending angle or morphing angle on the C_L and C_D .

There are two versions of the graph of the C_L . Figure 15 shows the original version of the C_L graph for trailing edge morphing, according to Fig. 3. In Fig. 15, the x -axis is the morphing angle, and the y -axis is the C_L , and each line represents the AOA. From this graph, able to identify how changing the bending angle affects the C_L at each AOA. Now

another graph in Fig. 16 shows similar data except the x -axis is the AOA and each line represents a bending angle. When compared to the graph in Fig. 15, this graph facilitates the comparison. The C_L results on the graph were assessed for each morphing distance to clearly understand the variation of morphing distance and other morphing parameters included in the graph in Fig. 16, which showed a clear pattern.

Individual evaluation of trailing edge morphing in NACA 2415 provided important and useful findings regarding morphing parameters. According to the results of the C_L , when the bending angle increases or bends clockwise, the C_L also increases. A review of the results reveals that the C_L of the positive trailing edge rose in comparison to the reference NACA 2415 airfoil, whereas the C_L of the negative trailing edge decreased. This tendency is noticeable for a range of attack angles, which are typically between -5° and 10° . As a result, when the wing is approaching stall, this occurrence is both significant and consistent. At this range, identifying the maximum and lowest coefficients will be easy and can be used to input probable wing shapes for the preferred flight

Fig. 15 C_L result plotted graph of NACA 2415 trailing edge at morphing length at 60% of chord location

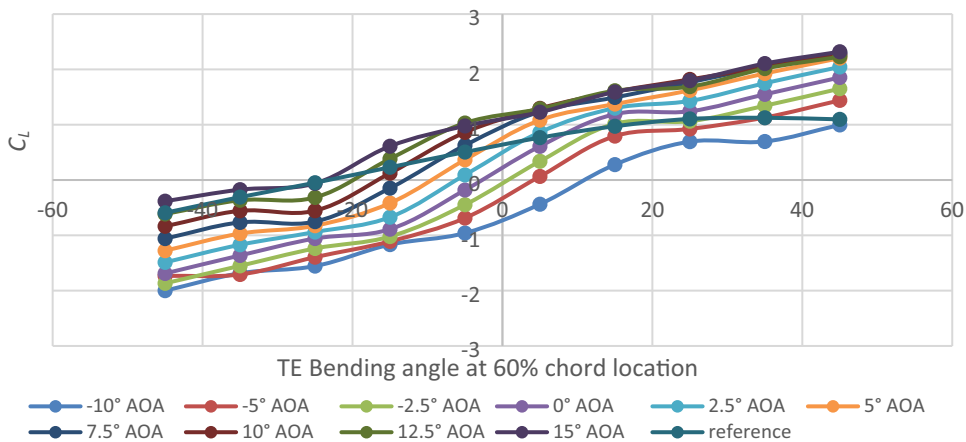
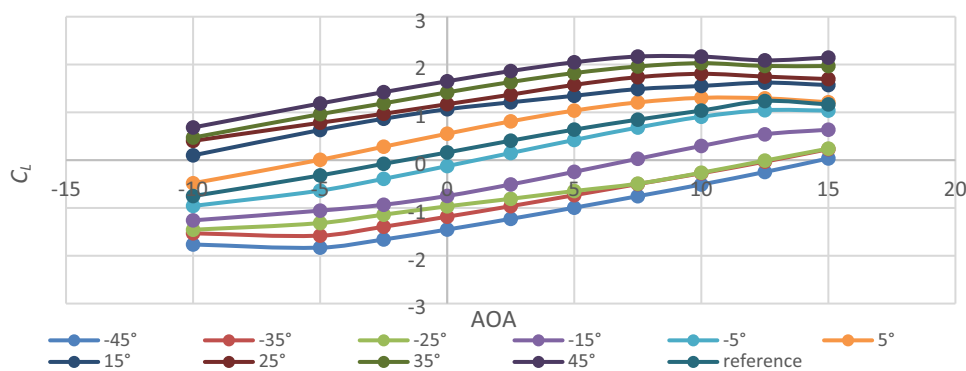


Fig. 16 NACA 2415 C_L results by AOA at 60% chords location for each trailing edge bending angle



phases, as shown in Table 4. This indicates that a satisfactory C_L can be achieved for a broad range of morphing bending angles.

Upon additional evaluation of trailing edge morphing bending, it was determined that position played a significant role in the C_L . Typically, the C_L of NACA 2415 for trailing edge morphing at a chord point of 50% was greater than at a chord location of 90%. Table 8 shows the percentage difference between trailing edge morphing at 90% chord location and other chord position comparisons at 90% chord location for 0° AOA and significant morphing bending angles. This makes it easier to select the wing designs with the optimum performance with an AOA of 0° for all chord points. All performance data for C_L for alternative wing designs were also analyzed.

The variation for the C_D result is very significant but decrease in C_D was found when morphing trailing edge bending took place. Figure 17 shows the C_D for morphing bending at 90% of the chord location for NACA 2415. Table 9 is used to measure the percentage difference in C_D based on morphing chord location.

To fully analyze the CD, Table 10 was formed to fully understand the percentage difference of the CD for all wing configurations and also the reduction of drag compared with the CFD reference. The design points that are highlighted in

Table 10 showed reduced CD. Due to induced drag caused by a finite wing, the CD is higher compared to the actual reference data [23, 25, 26]. Despite the induced drag, the negative percentage difference can be used to narrow the down-wing configuration for reduced drag. It will also be easier to narrow down the reduced drag required by the flight phases.

Subsequently, a CL/CD was measured to identify the design points or wing configurations significant for fuel usage. Table 11 shows the CL/CD for the AOA, and the highlighted design points show the increased CL/CD performance compared with the reference. Table 12 shows a similar table to Tables 8 and 9 to show the changes in the CL/CD ratio for morphing bending locations at 0°.

According to Table 10, the CD decreases when trailing edge bending occurs. At 0° of attack, the lower CD results are found for bending location when the chord location goes from 90 to 70%. For AOA above 0°, a lower CD can be achieved. Based on Table 10 drag improvement was found for wing configurations with trailing edge bending angles from - 5 to - 45°, but it is very significant when the TE bending angle is between - 5° and - 35° for all bending chord locations. Within that range, the CD increases significantly when the bending location changes.

Fig. 17 C_D result plotted graph of NACA 2415 trailing edge at morphing length at 90% of chord location

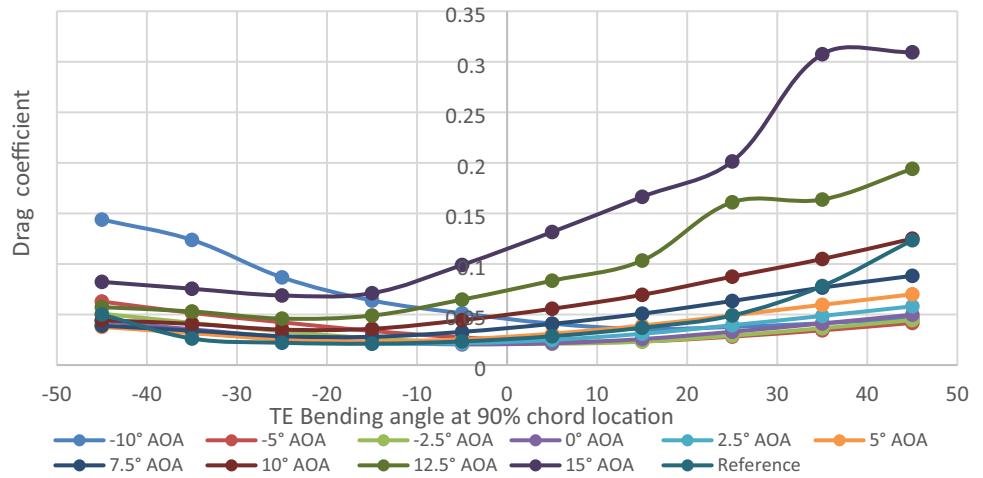


Fig. 18 C_L result plotted graph of NACA 0012 trailing edge at morphing length at 90% of chord location

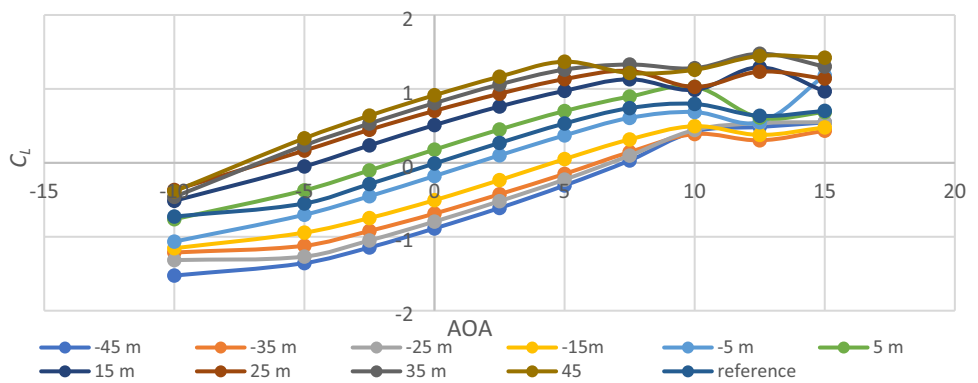
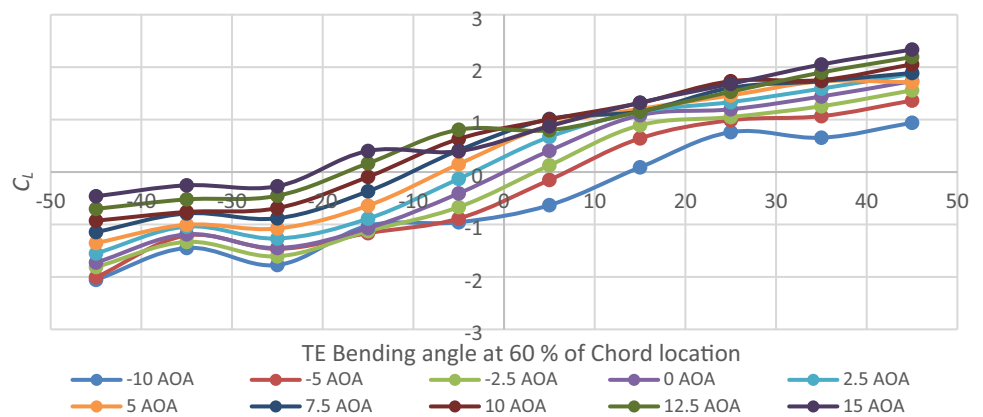


Fig. 19 C_L result plotted graph of NACA 0012 trailing edge at morphing length at 60% of chord location



Variation exists, however, in terms of the CL/CD ratio and position of morphing bending. Despite the complexity, all design points were evaluated based on each AOA location concerning the intended flight phase. Tables 8, 9, 10, 11, 12 are utilized to determine the ideal wing configuration for the chosen flight phase. For instance, in the cruise flight phase, according to Tables 3 and 4, wing configurations with reduced drag at zero AOA qualified as the ideal wing configurations for the cruise flight phase. Table 10 trailing edge

morphing of NACA 2415 wing configurations with a morphing bending angle of -5° and chord location ranging from 90 to 70% qualify for the cruise flight range, which consists of three wing configurations. Table 13 shows the optimal wing configurations of the trailing edge morphing of NACA 2415 for the cruise flight range, with an illustration of a morphing airfoil in Fig. 18.

Primarily, a significant increase in CL/CD will be considered to determine the potential wing configurations for

Fig. 20 C_D result plotted graph of NACA 0012 trailing edge at morphing length at 50% of chord location

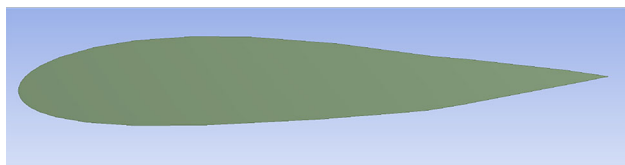
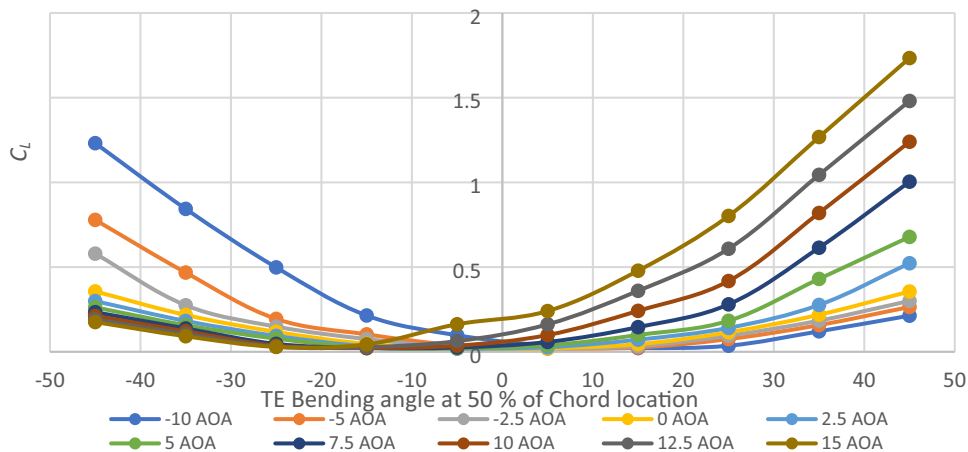


Fig. 21 NACA 2415 morphing trailing edge length at 70% of chord for -5° bending angle

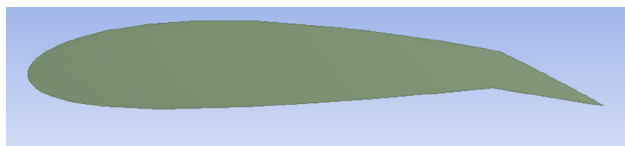


Fig. 22 NACA 2415 trailing edge morphing length at 80% of chord for 15° bending angle

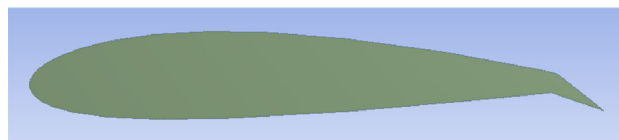


Fig. 23 NACA 2415 trailing edge morphing length at 90% of chord for 25° bending angle

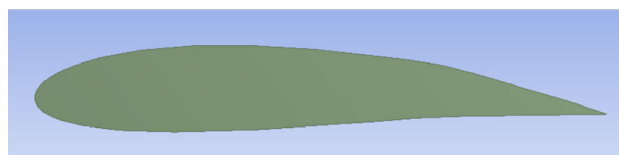


Fig. 24 NACA 2415 trailing edge morphing length at 70% of chord for 5° bending angle

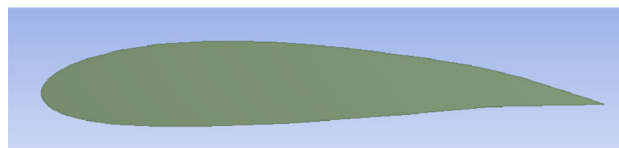


Fig. 25 NACA 2415 trailing edge morphing length at 80% of chord for 5° bending angle

NACA 2415 trailing edge morphing, providing optimal performance for the climbing phase. Table 14 shows all the optimal wing configurations for the climbing flight phase. Figures 19, 20, 21, 22, 23, 24, 25 show wing configurations showing optimal C_L/C_D performance at each AOA, providing significant climbing flight-phase improvement.

For the take-off phase of flight, the maximum takeoff angle can range from 10° to 15° . Assessing Tables 10 and 11 for the increased C_L/C_D , followed by lower drag to allocate the optimal wing configuration for optimal take-off performance. Having these two criteria will reduce takeoff distance, lower fuel consumption, and provide a quicker and more reliable takeoff. Table 15 displays the best NACA 2415 trailing edge morphing wing configurations for the take-off flight phase.

For the descending and landing flight phases, the requirement is an increase in C_D and a negative C_L . Based on the C_L assessment, when the trailing edge bending goes anticlockwise, the C_L decreases, as shown in Figs. 15 and 16, and the C_D increases as well. For AOA below 0° , all the wing configurations of the NACA 2415 trailing edge morphing bending

angle range from -5° to -45° and are also applicable for all trailing edge bending locations. Overall, optimal NACA 2415 trailing edge morphing wing configurations for optimal flight performance were identified.

5.2 Trailing Edge Morphing for Symmetric Airfoil NACA 0012

Similarly, a CFD experiment was conducted on NACA 0012 for the trailing edge morphing concept. For the same range of attack angles, the C_L and C_D both increased and decreased in a similar pattern. Figures 26 and 27 demonstrate that the C_L

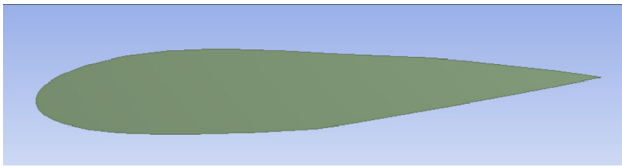


Fig. 26 NACA 2415 trailing edge morphing length at 50% of chord for -5° bending angle

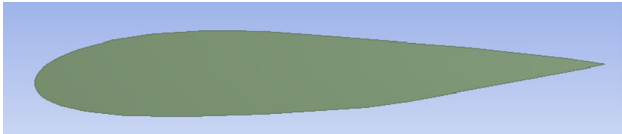


Fig. 27 NACA 2415 trailing edge morphing length at 60% of chord for -5° bending angle

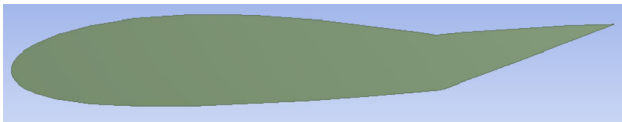


Fig. 28 NACA 2415 trailing edge morphing length at 70% of chord for -5° bending angle

findings for the two C_L graph types are comparable, while Fig. 28 shows the C_D results. However, the fluctuation of the C_L began when the AOA exceeded 5° . The NACA 0012 airfoil was evaluated similarly for each AOA at each morphing location (see Tables 8, 9, and 13). The effect of the morphing bending angle and morphing location is identical to that of NACA 2415.

To determine the best wing configuration for the NACA 0012 during preferred flight phases, percentage differences in C_D and C_L/C_D are calculated, along with other assessments similar to the NACA 2415. Table 16 displays the percentage differences in C_D results when compared to the reference CFD NACA 0012 data. Identifying the aerodynamically optimal wing configuration, Table 17 shows the C_L/C_D ratio compared with the reference NACA 0012.

After analyzing the entire data set, the optimal wing configurations for NACA 0012 trailing edge morphing were identified. According to Table 18, there is no improvement in C_D for cruise flight when it comes to trailing edge bending and morphing location. The C_D significantly increased despite the increase in C_L , therefore the NACA 2415, which is an asymmetric airfoil, showed better cruise performance compared to the NACA 0012. This proves that trailing edge morphing for the cruise flight phase, NACA 2415 is preferred over NACA 0012.

But despite this case, the optimal wing configuration for NACA 0012 was identified for climbing flight and takeoff flight phases using similar assessments used for NACA 2415



Fig. 29 NACA 0012 trailing edge morphing length at 90% of chord for 5° bending angle

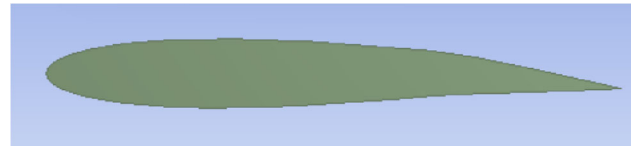


Fig. 30 NACA 0012 trailing edge morphing length at 70% of chord for 5° bending angle



Fig. 31 NACA 0012 trailing edge morphing length at 80% of chord for -5° bending angle



Fig. 32 NACA 0012 trailing edge morphing length at 60% of chord for -5° bending angle

trailing edge morphing wings, as shown in Tables 19 and 20, respectively. For the climbing flight phase, increments of C_L/C_D ratio were used to identify optimal wing configurations for the flight, and for the takeoff flight phase, both C_L/C_D and C_D were considered to determine the optimal designs of the NACA 0012 trailing edge morphing wing. Also, for the descending and landing flight phases, NACA 0012 showed a similar pattern, with all the wing configurations of NACA 0012 having a trailing edge morphing bending angle ranging from -5° to -45° and applicable for all trailing edge bending locations. Figures 19, 20, 21, 22, 23, 24, 25 show wing configurations showing optimal C_L/C_D performance at each AOA, providing significant climbing flight-phase improvement.

The trailing edge morphing concept appeared to have some similarities and differences between asymmetrical and symmetrical airfoils. The asymmetric NACA 2415 trailing edge morphing modification has a positive impact on the cruising flight phase because the C_D is reduced at 0° AOA. Based on Table 21, a comparison was made between the symmetric and asymmetric airfoils chosen for this research.



Fig. 33 NACA 0012 trailing edge morphing length at 50% of chord for -5° bending angle

Overall, trailing edge morphing on a trailing edge is preferred for asymmetric airfoils compared to symmetric airfoils. But in terms of climbing, descending, takeoff, and landing flight phases, both types of airfoils are suitable.

6 Conclusion

NACA 2415 showed lower C_D results for trailing edge bending at 0° of attack at morphing bending locations from 90 to 70% of the chord, improving cruise flight phase overall. NACA 2415 had the best cruise flight wing configurations with a morphing bending angle of -5° and bending location of 90–70% of the chord. NACA 2415 was better for this phase because NACA 0012 did not improve C_D . For climb and takeoff flight performance improvement, trailing edge morphing wings with better C_L/C_D at each AOA

improved climbing flight. Trailing edge morphing configurations identified optimal takeoff wing configurations with increased C_L/C_D and lower drag. Possible and improved landing flight phase C_L results dropped when the trailing edge bent anticlockwise, which meets descending and landing flight-phase requirements for increased C_D and decreased C_L . The optimal configurations and aerodynamic performance, the extensive CFD simulations (over 1000 design points) showed the potential to save time and money in the design process. Similar CFD or wind tunnel testing methods are recommended for other airfoils. Morphing wing design using X-FOIL, JavaFoil, or other computer-aided design software and basing length or position on wing chord length can save time and money. Findings on aerodynamic-performance enhancements can help implement trailing edge morphing technology in conventional wings for fuel-efficient commercial and civil aircraft.

Appendix: Tables

See Tables 1, 2, 3, 4, 5, 6, 7, 8, 9, 10, 11, 12, 13, 14, 15, 16, 17, 18, 19, 20, 21.

Table 1 Key finding of wind-tunnel the experiment of morphed FX63-137 at $Re = 1 \times 10^6$

Angle of attack (Deg.)	Morphing angle θ showed improved performance than the reference value	Morphing angle showed lower C_L performance than the reference value	Estimated maximum percentage of C_L improvement	The minimum percentage of C_L reduced
0	$\theta > 13$	$0 < \theta < 13$	25%	Below 10%
5	$\theta > 12$	$0 < \theta < 12$	35%	Below 10%
10	$\theta > 10$	None	15%	none
16	None	None	None	None
20	None	None	None	none

Table 2 Equation and theories relating lift and drag coefficients to aerodynamic measures based on three flight phases considered

Flight phase	Equation and aspect significant to optimal performance	Impact and implications	References
Take off	<p>Equation (5) shows Stall velocity (V_s), the minimum velocity required for the aircraft to take off. For this stage, we can assume the minimum force required to overcome is the weight, (W) of the aircraft which is equal to lift force in Eq. (1), also, rotational stall velocity follows the same equation where maximum lift coefficient, (C_{LMAX}) is a factor and density of air (ρ) and reference area (A), remain constant</p> <p>Generally, the equation of stall velocity is:</p> $V_s = \sqrt{\frac{2W}{\rho AC_{LMAX}}} \quad (5)$ <p>Total take-off distance or take-off range depends on the stall velocity required for take-off</p>	<p>An increase in C_{LMAX} reduces stall velocity</p> <p>Changes in stall velocity also affect the take-off distance required overall</p>	[28]
Climbing	<p>Considering steady climb conditions, the thrust required (T) is the combination of weight and drag forces components, (D_{comp}) and (W_{comp}) based on the climbing angle. In general terms total Thrust T required in Eq. (6):</p> $T = D_{comp} + W_{comp} \quad (6)$ <p>To make it simpler we can transform the equation after using the component of each force to identify the specific excess power required (P_s) for the climbing flight phase in Eq. (7):</p> $P_s = \frac{(T-D)V}{W} \quad (7)$ <p>Climb power is significant to climb the distance required</p>	<p>Lower C_D reduces the thrust required and has a good impact on climbing power. Better C_L/C_D also improves the climbing power and increases payload effectively</p>	[28, 29]
Cruise	<p>For steady-flight conditions at velocity (V), thrust required for the cruise is equal to drag force in Eq. (2)</p> <p>Based on the thrust force and for a specific fuel consumption power ($Fuel_{constant}$) and constant fuel load (M), Eqs. (8) and (9) show how to determine the maximum flight duration (t_{max}) and maximum flight range (R) respectively:</p> $t_{max} = \frac{M}{Fuel_{constant} T} \quad (8)$ $R = V \times t_{max} \quad (9)$	<p>The drag coefficient impacts the thrust force required during the cruise. Since changing the thrust force impacts the flight time, it also changes the flight range</p>	[30, 31]

Table 3 Requirement of lift and drag coefficient by morphing wing configuration and its impact on aerodynamic performance and economic value

Flight phases	C_L and C_D changes are required for optimal performance by morphing configuration	The overall impact on performance compared to a regular fixed wing	Economic value
Take-off	Reduction of C_D Increase of C_L/C_D Increase of C_{LMAX}	Reducing stall velocity Reduces take-off distance	Less stall velocity and reduced take-off distance would lower fuel consumption and Quicker and more reliable take-off [28, 29]
Climbing	Increased C_L/C_D Reduction of C_D	Reduces the thrust required hence climb power is reduced and shorter climb distance to cruise	Less thrust means less fuel power required for an effective powerful climb and shorter climb distance means a quicker climb can be achieved. For the same climbing power, either more payload can be increased or a shorter climb can be achieved [29, 32]
Cruise	Reduction of C_D and increase of C_L/C_D at cruise	Increase flight duration time and flight range	Longer flight range means more distance covered for the same amount of fuel. Also, less fuel is consumed if we consider a fixed flight range during the cruise [30, 31]
Decent and landing	Increase of C_D Reduction of negative C_L	Enhancing reliable landing performance	Landing flight phase is a dangerous phase of flight, it is important to aim for reliable landing compared to achieving enhanced landing performance. Reliable and safe landing, providing time-efficient landing and decent flight phases [28, 33]

Table 4 Percentage difference requirements of the aerodynamic results of morphing airfoil compared to reference airfoil for each flight phase

Required by flight phase	AOA	Highest positive Cl difference	Highest negative CD difference	Highest positive CD difference required	Highest positive CL/CD required
Cruise	At 0° angle of attack	Not required	Required	Not required	Not required
Take-off	Stall angle range	Secondary	Primary	Not required	Primary
Climbing	Stall angle range	Secondary	Secondary	Not required	Primary
Decent and landing	Stall angle range	Not required	Not required	Primary	Not required

Table 5 Tabulated result of C_L result of fluent verification NACA 2415 at Reynolds number 303100

AOA/°	C_L from reference data for NACA2415 [23]	C_L from CFD simulation	Percentage difference (%)
- 4.87°	- 0.263	- 0.30522	4.22
- 3.43°	- 0.139	- 0.16769	2.87
- 1.79°	0.017	- 0.01041	2.74
- 0.29°	0.165	0.161737	0.33
1.25°	0.344	0.318106	2.59
2.82°	0.541	0.479688	6.13
4.35°	0.72	0.629845	9.02
5.87°	0.853	0.785902	6.71
7.41°	0.96	0.925433	3.46
8.92°	1.051	1.060511	- 0.95
10.44°	1.13	1.191561	- 6.16

Table 6 New reference data for NACA 2415 3D wing

AOA/°	C_L from CFD simulation for reference point	C_D from CFD simulation for reference point
- 10°	- 0.5927	0.0500
- 5°	- 0.3090	0.0262
- 2.5°	- 0.0495	0.0221
0°	0.2304	0.0211
2.5°	0.5052	0.0234
5°	0.7661	0.0285
7.5°	0.9720	0.0369
10°	1.1042	0.0490
12.5°	1.1249	0.0782
15°	1.0964	0.1235

Table 7 New reference data for NACA 0012 3D wing

AOA	C_L from CFD simulation for reference point	C_D from CFD simulation for reference point
- 10°	- 0.7265	0.0984
- 5°	- 0.5496	0.0224
- 2.5°	- 0.2864	0.0169
0°	- 0.0083	0.0153
2.5°	0.2695	0.0169
5°	0.5324	0.0224
7.5°	0.7400	0.0339
10°	0.7967	0.1342
12.5°	0.6364	0.1217
15°	0.7031	0.2304

Table 8 Percentage difference of C_L for NACA 2415 trailing edge morphing bending angle compared to 90% chord location at 0° AOA

Trailing edge morphing location/type of data compared with (%)	Data compared with	Morphing bending angle						
		- 25 (%)	- 15 (%)	- 5 (%)	5 (%)	15 (%)	25 (%)	35 (%)
90	(Compared with reference data)	- 302	- 217	- 79	67	194	267	329
80	90 chord location	69	104	- 205	25	33	25	26
70	90 chord location	108	177	- 353	44	57	38	44
60	90 chord location	128	229	- 469	58	76	47	57
50	90 chord location	145	270	- 565	70	90	53	68

Table 9 Percentage difference of C_D for trailing edge morphing bending angle compared to 90% chord location at 0°

Trailing edge morphing location/type of data compared with (%)	Data compared with	Morphing bending angle						
		- 25 (%)	- 15 (%)	- 5 (%)	5 (%)	15 (%)	25 (%)	35 (%)
90	(Compared with CFD reference data)	32	7	- 3	2	22	56	95
80	90 chord location	44	14	1	4	22	52	70
70	90 chord location	100	32	2	8	45	112	160
60	90 chord location	169	53	4	11	69	191	283
50	90 chord location	258	75	5	14	93	291	446

Table 10 Percentage difference of C_D results for NACA 2415 trailing edge morphing

AOA/°	Morphing Bending angle/°									
	45	-35	-25	-15	-5	5	15	25	35	45
-10	188%	148%	73%	28%	2%	-18%	-29%	-25%	-17%	-7%
-5	139%	97%	61%	29%	4%	-9%	-11%	7%	31%	59%
-2.5	130%	89%	51%	20%	1%	-4%	5%	32%	65%	102%
0	106%	68%	32%	7%	-3%	2%	22%	56%	95%	136%
2.5	67%	37%	9%	-8%	-8%	6%	32%	69%	108%	148%
5	32%	11%	-11%	-18%	-10%	9%	37%	73%	109%	146%
7.5	5%	-8%	-23%	-24%	-11%	10%	38%	72%	108%	139%
10	-9%	-17%	-28%	-27%	-9%	14%	42%	78%	114%	155%
12.5	-27%	-32%	-41%	-37%	-17%	7%	32%	106%	110%	148%
15	-33%	-39%	-44%	-42%	-20%	7%	35%	63%	149%	151%
-10	390%	243%	140%	133%	8%	-23%	-39%	-21%	10%	41%
-5	323%	223%	135%	60%	10%	-12%	-6%	52%	121%	195%
-2.5	324%	217%	122%	45%	4%	-4%	20%	101%	184%	278%
0	286%	183%	91%	22%	-2%	6%	49%	137%	232%	335%
2.5	214%	126%	47%	-4%	-10%	13%	67%	151%	243%	343%
5	139%	73%	2%	-23%	-15%	17%	73%	147%	233%	323%
7.5	76%	25%	-26%	-34%	-18%	19%	71%	138%	218%	301%
10	30%	-5%	-41%	-38%	-17%	22%	68%	149%	243%	367%
12.5	-17%	-35%	-55%	-46%	-26%	18%	49%	172%	217%	299%
15	-42%	-47%	-62%	-47%	-25%	14%	50%	141%	239%	311%
-10	917%	598%	251%	103%	19%	-28%	-45%	-10%	54%	125%
-5	608%	393%	217%	101%	17%	-14%	0%	106%	239%	386%
-2.5	593%	380%	207%	75%	9%	-4%	37%	176%	336%	523%
0	527%	328%	165%	41%	-1%	10%	77%	231%	408%	612%
2.5	405%	236%	99%	4%	-12%	19%	104%	249%	417%	615%
5	275%	146%	35%	-23%	-19%	24%	113%	242%	396%	573%
7.5	167%	74%	-18%	-39%	-22%	27%	110%	226%	366%	536%
10	89%	27%	-43%	-47%	-21%	33%	109%	231%	380%	577%
12.5	11%	-22%	-62%	-56%	-29%	27%	90%	228%	383%	609%
15	-32%	-50%	-71%	-59%	-30%	29%	84%	240%	347%	520%
-10	1373%	914%	374%	202%	29%	-32%	-48%	-4%	111%	233%
-5	1529%	628%	333%	151%	23%	-16%	9%	177%	388%	641%
-2.5	971%	597%	317%	114%	13%	-3%	55%	274%	540%	857%
0	862%	521%	256%	63%	1%	13%	106%	354%	647%	998%
2.5	669%	386%	171%	16%	-13%	24%	146%	379%	663%	997%
5	468%	250%	91%	-19%	-21%	31%	165%	365%	628%	926%
7.5	298%	141%	-4%	-40%	-26%	36%	160%	343%	596%	871%
10	173%	65%	-39%	-51%	-26%	46%	150%	361%	651%	987%
12.5	56%	-7%	-64%	-63%	-35%	38%	137%	426%	605%	975%
15	-8%	-45%	-76%	-68%	-32%	38%	123%	353%	540%	743%
-10	1979%	1254%	672%	341%	42%	-35%	-49%	7%	184%	383%
-5	1853%	969%	487%	213%	29%	-17%	19%	243%	583%	992%
-2.5	1466%	907%	455%	162%	17%	-2%	74%	408%	804%	1313%
0	1308%	782%	374%	87%	2%	16%	136%	510%	965%	1518%
2.5	1021%	578%	269%	30%	-13%	30%	209%	551%	992%	1517%
5	721%	382%	129%	-13%	-23%	38%	234%	530%	932%	1410%
7.5	464%	223%	14%	-40%	-29%	45%	220%	492%	869%	1317%
10	282%	113%	-33%	-54%	-30%	59%	208%	516%	947%	1777%
12.5	115%	21%	-64%	-67%	-40%	45%	176%	584%	942%	1365%
15	22%	-35%	-78%	-73%	-38%	40%	151%	444%	718%	1022%
	=	Morphing bending location at 90% of chord location								
	=	Morphing bending location at 80% of chord location								
	=	Morphing bending location at 70% of chord location								
	=	Morphing bending location at 60% of chord location								
	=	Morphing bending location at 50% of chord location								
X%	=	Reduction of C_D at low range by X%								
X%	=	Reduction of C_D at medium range by X%								
X%	=	Reduction of C_D at high range by X%								

Table 11 Percentage difference of C_L/C_D for trailing edge morphing of NACA 2415

AOA/°	Morphing Bending angle/°									
	45	-35	-25	-15	-5	5	15	25	35	45
0	-249%	-253%	-252%	-210%	-78%	64%	141%	135%	120%	100%
2.5	-148%	-143%	-135%	-100%	-31%	22%	39%	30%	19%	8%
5	-109%	-99%	-88%	-57%	-15%	8%	10%	1%	-7%	-15%
7.5	-76%	-64%	-53%	-30%	-5%	4%	1%	-8%	-18%	-23%
10	-41%	-30%	-29%	-12%	1%	1%	-5%	-17%	-26%	-38%
12.5	11%	16%	-1%	20%	17%	6%	-2%	-31%	-30%	-39%
15	26%	38%	14%	38%	20%	6%	-6%	-5%	-46%	-39%
0	-229%	-247%	-278%	-297%	-123%	97%	163%	94%	63%	42%
2.5	-156%	-162%	-177%	-161%	-51%	30%	31%	1%	-15%	-26%
5	-134%	-134%	-147%	-104%	-24%	9%	-3%	-21%	-34%	-43%
7.5	-120%	-115%	-119%	-61%	-6%	1%	-12%	-28%	-40%	-48%
10	-104%	-90%	-82%	-27%	5%	-4%	-14%	-37%	-52%	-65%
12.5	-71%	-44%	-28%	15%	30%	-7%	-6%	-48%	-48%	-55%
15	0%	25%	17%	32%	32%	10%	-4%	-41%	-52%	-57%
0	-200%	-220%	-258%	-331%	-154%	119%	162%	53%	21%	1%
2.5	-148%	-157%	-180%	-197%	-66%	35%	17%	-22%	-37%	-48%
5	-135%	-139%	-162%	-141%	-32%	9%	-17%	-40%	-52%	-60%
7.5	-129%	-130%	-162%	-95%	-10%	-2%	-27%	-45%	-57%	-65%
10	-124%	-120%	-142%	-50%	5%	-11%	-33%	-51%	-62%	-71%
12.5	-120%	-104%	-102%	10%	31%	-9%	-24%	-53%	-64%	-74%
15	-95%	-58%	-24%	42%	36%	-15%	-22%	-54%	-60%	-68%
0	-176%	-195%	-229%	-336%	-178%	134%	151%	19%	-10%	-27%
2.5	-138%	-148%	-169%	-215%	-79%	38%	4%	-41%	-55%	-63%
5	-129%	-136%	-156%	-167%	-39%	7%	-32%	-55%	-65%	-72%
7.5	-127%	-133%	-181%	-125%	-13%	-7%	-41%	-59%	-70%	-76%
10	-128%	-131%	-183%	-77%	6%	-20%	-42%	-64%	-75%	-81%
12.5	-135%	-135%	-178%	-8%	41%	-17%	-39%	-71%	-75%	-82%
15	-138%	-129%	-123%	74%	31%	-19%	-35%	-64%	-70%	-75%
0	-159%	-174%	-204%	-332%	-197%	143%	137%	-8%	-32%	-45%
2.5	-130%	-138%	-155%	-222%	-90%	38%	-14%	-55%	-66%	-73%
5	-124%	-130%	-156%	-184%	-45%	6%	-45%	-66%	-74%	-80%
7.5	-124%	-130%	-187%	-150%	-16%	-11%	-53%	-69%	-77%	-82%
10	-127%	-131%	-206%	-103%	6%	-27%	-53%	-73%	-81%	-89%
12.5	-138%	-143%	-236%	-34%	49%	-22%	-47%	-76%	-82%	-85%
15	-152%	-162%	-228%	69%	54%	-20%	-40%	-68%	-75%	-80%
	=	Morphing bending location at 90% of chord location								
	=	Morphing bending location at 80% of chord location								
	=	Morphing bending location at 70% of chord location								
	=	Morphing bending location at 60% of chord location								
	=	Morphing bending location at 50% of chord location								
X%	=	Showing positive or increased C_L/C_D by X%								

Table 12 Percentage difference of C_L/C_D for NACA 2415 trailing edge morphing bending angle compared to 90% chord location at 0° AOA

Trailing edge morphing location/type of data compared with (%)	Data compared with	Morphing bending angle						
		- 25 (%)	- 15 (%)	- 5 (%)	5 (%)	15 (%)	25 (%)	35 (%)
90	(Compared with reference data)	- 252	- 210	- 78	64	141	135	120
80	90% chord location	17	79	- 204	20	9	- 18	- 26
70	90% chord location	4	110	- 347	33	9	- 35	- 45
60	90% chord location	- 15	115	- 456	43	4	- 49	- 59
50	90% chord location	- 32	111	- 541	48	- 2	- 61	- 69

Table 13 Optimal wing configuration of NACA 2415 trailing edge morphing for cruise flight phase

AOA	Percentage of drag reduction (%)	Morphing Location	Bending angle	Wing design example
0	- 3	90	- 5°	Figure 21
0	- 2	80	- 5°	
0	- 1	70	- 5°	

Table 14 Optimal wing configuration of NACA 2415 trailing edge morphing for climbing flight phase

AOA	Range of increased C_L/C_D /%	Morphing location/% of chord location (%)	No of designs	Bending angles/angle range showing optimal performance	Wing design example of optimal performance for a specific AOA
0	64–141	90	5	5° till 45°	Figure 22
	42–163	80	5	5° till 45°	
	1–162	70	5	5° till 35°	
	19–134	60	3	5° till 25°	
	143–137	50	2	5° and 15°	
2.5	8–39	90	5	5° till 45°	FIGURE 23
	1–31	80	3	5° till 25°	
	35 and 17	70	2	5° and 15°	
	38 and 4	60	2	5° and 15°	
	38	50	1	5°	
5	1–10	90	3	5° till 25°	Figure 24
	9	80	1	5°	
	9	70	1	5°	
	7	60	1	5°	
	6	50	1	5°	
7.5	4 and 1	90	2	5° and 15°	Figure 25
	1	80	1	5°	
10	1	90	2	- 5° and 5°	Figure 26
	5	80	1	- 5°	
	5	70	1	- 5°	
	6	60	1	- 5°	
	6	50	1	- 5°	
12.5	8–20	90	5	- 45°, - 35° and - 15° till 5°	Figure 27
	15 and 30	80	2	- 15° and - 5°	
	10 and 31	70	2	- 15° and - 5°	
	41	60	1	- 5°	
	49	50	1	- 5°	
15	6–38	90	6	- 45° till 5°	Figure 28
	10–32	80	5	- 35° till 5°	
	42 and 36	70	2	- 15° and - 5°	
	74 and 31	60	2	- 15° and - 5°	
	69 and 54	50	2	- 15° and - 5°	

Table 15 Optimal wing configuration of NACA 2415 trailing edge morphing for take-off flight phase

AOA	Percentage of drag reduction (%)	Percentage of increased C_L/C_D (%)	Morphing location/% of chord location	Number of wing designs	Bending angles showing optimal performance	Wing design reference of optimal performance for a specific AOA
10	- 9	1	90	1	- 5°	Figure 18
	- 17	5	80	1	- 5°	
	- 21	5	70	1	- 5°	
	- 26	6	60	1	- 5°	
	- 30	6	50	1	- 5°	
12.5	- 17	17	90	4	- 5°	Figure 23
	- 37,	20			- 15°	
	- 32	16			- 35°	
	- 27	11			- 45°	
	- 46	30	80	2	- 5°	
	- 26	15			- 15°	
	- 56	31	70	2	- 5°	
	- 29	10			- 15°	
	- 35	41	60	1	- 5	
	- 40	49	50	1	- 5	
15	- 20	20	90	5	- 5°	Figure 25
	- 42	38			- 15°	
	- 44	14			- 25°	
	- 39	38			- 35°	
	- 33	26			- 45°	
	- 25	32	80	4	- 5°	
	- 47	32			- 15°	
	- 62	17			- 25°	
	- 47	25			- 35°	
	- 30	36	70	2	- 5°	
	- 59	42			- 15°	
	- 32	31	60	2	- 5°	
	- 68	74			- 15°	
- 38	54	50	2	- 5°		
- 73	69			- 15°		

Table 16 Percentage difference of C_D for trailing edge morphing of NACA 0012

AOA ^o	Morphing Bending angle/ ^o									
	-45	-35	-25	-15	-5	5	15	25	35	45
-10	138%	130%	65%	55%	-33%	-49%	-60%	-60%	-50%	-38%
-5	236%	120%	163%	72%	31%	5%	-4%	11%	46%	82%
-2.5	238%	117%	169%	67%	31%	14%	18%	52%	102%	155%
0	209%	93%	145%	46%	24%	24%	46%	95%	154%	217%
2.5	147%	53%	96%	19%	15%	31%	66%	121%	182%	249%
5	76%	11%	42%	-4%	6%	31%	68%	124%	186%	247%
7.5	20%	-15%	0%	-18%	-3%	24%	59%	181%	219%	341%
10	-62%	-70%	-68%	-70%	-54%	-45%	-31%	17%	113%	73%
12.5	-17%	-35%	-45%	-5%	-22%	26%	65%	67%	162%	199%
15	-25%	-45%	-51%	-49%	24%	-10%	4%	40%	77%	100%
-10	302%	166%	91%	111%	-21%	-53%	-67%	-68%	-47%	-30%
-5	1261%	346%	224%	123%	41%	-1%	-7%	51%	142%	229%
-2.5	533%	369%	231%	112%	38%	12%	31%	131%	251%	374%
0	490%	332%	198%	77%	27%	27%	77%	202%	341%	488%
2.5	374%	244%	133%	31%	12%	39%	112%	242%	380%	520%
5	229%	136%	43%	-7%	-1%	41%	119%	245%	363%	482%
7.5	105%	48%	-18%	-31%	-10%	33%	106%	311%	430%	448%
10	-49%	-62%	-77%	-76%	-63%	-43%	0%	114%	147%	198%
12.5	-36%	-51%	-65%	-56%	-27%	4%	84%	181%	241%	333%
15	-42%	-55%	-68%	-48%	20%	-9%	39%	96%	143%	196%
-10	513%	286%	201%	63%	-13%	-57%	-72%	-69%	-30%	5%
-5	1299%	876%	363%	185%	51%	-5%	-3%	94%	260%	432%
-2.5	926%	618%	377%	169%	46%	11%	50%	222%	427%	671%
0	858%	563%	321%	111%	30%	31%	116%	333%	564%	876%
2.5	673%	426%	212%	48%	11%	46%	175%	386%	622%	983%
5	431%	255%	98%	-3%	-5%	50%	190%	390%	583%	1025%
7.5	223%	114%	-4%	-35%	-18%	45%	365%	415%	722%	971%
10	-24%	-49%	-78%	-80%	-68%	-40%	51%	133%	264%	323%
12.5	-20%	-45%	-74%	-59%	-28%	28%	109%	259%	378%	549%
15	-56%	-67%	-79%	-64%	-2%	-5%	60%	145%	224%	325%
-10	804%	298%	534%	122%	-3%	-60%	-76%	-68%	-7%	52%
-5	1932%	951%	1369%	267%	61%	-8%	4%	153%	404%	700%
-2.5	1890%	576%	971%	246%	54%	11%	68%	317%	658%	1086%
0	1436%	476%	876%	153%	34%	34%	148%	478%	888%	1417%
2.5	1099%	327%	665%	70%	11%	53%	234%	578%	1010%	1574%
5	711%	159%	409%	4%	-8%	59%	253%	556%	1003%	2251%
7.5	387%	50%	204%	-36%	-22%	59%	249%	522%	1028%	2059%
10	13%	-77%	-30%	-82%	-71%	-19%	77%	173%	354%	569%
12.5	16%	-76%	-32%	-73%	-20%	51%	147%	320%	567%	809%
15	-42%	-86%	-65%	-61%	-32%	-2%	84%	191%	336%	472%
-10	1151%	757%	406%	118%	-1%	-63%	-78%	-63%	23%	117%
-5	3371%	1985%	766%	360%	71%	-10%	14%	235%	603%	1080%
-2.5	3323%	1524%	778%	344%	60%	11%	93%	460%	986%	1674%
0	2232%	1322%	670%	207%	38%	38%	196%	655%	1330%	2227%
2.5	1670%	978%	456%	96%	12%	60%	324%	736%	1536%	2992%
5	1070%	601%	247%	14%	-11%	69%	343%	716%	1818%	2924%
7.5	590%	307%	39%	-35%	-25%	71%	329%	725%	1710%	2859%
10	58%	-10%	-73%	-83%	-73%	-26%	80%	211%	511%	824%
12.5	58%	-13%	-75%	-77%	-48%	33%	196%	400%	758%	1117%
15	-24%	-60%	-87%	-81%	-29%	4%	108%	248%	450%	652%
	=	Morphing bending location at 90% of chord location								
	=	Morphing bending location at 80% of chord location								
	=	Morphing bending location at 70% of chord location								
	=	Morphing bending location at 60% of chord location								
	=	Morphing bending location at 50% of chord location								
X%	=	Reduction of C_D at low range by X%								
X%	=	Reduction of C_D at medium range by X%								
X%	=	Reduction of C_D at high range by X%								

Table 17 Percentage difference of C_L/C_D for trailing edge morphing of NACA 0012

AOA/°	Morphing Bending angle/° for NACA 0012									
	-45	-35	-25	-15	-5	5	15	25	35	45
2.5	-192%	-203%	-198%	-173%	-67%	27%	71%	57%	39%	24%
5	-133%	-125%	-130%	-90%	-34%	0%	9%	-5%	-17%	-26%
7.5	-96%	-77%	-87%	-48%	-15%	-3%	-4%	-40%	-44%	-63%
10	42%	62%	74%	105%	86%	134%	80%	10%	-24%	-8%
12.5	-8%	-26%	53%	-37%	11%	-24%	23%	16%	-11%	-24%
15	3%	13%	60%	33%	35%	9%	32%	16%	5%	1%
2.5	-180%	-195%	-222%	-248%	-99%	45%	70%	22%	2%	-10%
5	-144%	-150%	-173%	-150%	-47%	4%	-5%	-31%	-40%	-46%
7.5	-133%	-133%	-157%	-94%	-20%	-3%	-19%	-57%	-59%	-55%
10	-146%	-120%	-145%	54%	144%	107%	31%	-34%	-13%	-37%
12.5	-53%	-7%	-22%	53%	53%	-7%	-16%	-29%	-31%	-38%
15	48%	-46%	-25%	8%	13%	38%	20%	-2%	-5%	-13%
2.5	-163%	-177%	-212%	-283%	-124%	56%	42%	-6%	-23%	-42%
5	-139%	-146%	-178%	-191%	-59%	5%	-27%	-48%	-54%	-69%
7.5	-136%	-142%	-196%	-140%	-23%	-7%	-70%	-60%	-72%	-75%
10	-199%	-203%	-368%	-49%	165%	106%	-14%	-37%	-41%	-47%
12.5	-163%	-144%	-220%	-5%	-2%	30%	-23%	-39%	-44%	-53%
15	-83%	-18%	-60%	16%	62%	31%	5%	-12%	-19%	-30%
2.5	-148%	-191%	-161%	-294%	-143%	62%	27%	-27%	-47%	-59%
5	-131%	-173%	-140%	-216%	-69%	5%	-36%	-58%	-71%	-86%
7.5	-132%	-171%	-139%	-178%	-28%	-14%	-55%	-65%	-79%	-88%
10	-203%	-508%	-224%	-165%	170%	55%	-7%	-20%	-51%	-61%
12.5	-195%	-442%	-204%	-4%	59%	-17%	-27%	-43%	-55%	-62%
15	-213%	-351%	-209%	47%	-17%	27%	2%	-18%	-33%	-42%
2.5	-137%	-148%	-176%	-290%	-158%	65%	3%	-38%	-62%	-76%
5	-126%	-133%	-159%	-228%	-78%	3%	-49%	-65%	-83%	-87%
7.5	-128%	-135%	-210%	-205%	-33%	-18%	-64%	-74%	-87%	-90%
10	-196%	-221%	-560%	-276%	180%	67%	-4%	-38%	-60%	-69%
12.5	-201%	-228%	-577%	-76%	138%	4%	-33%	-48%	-62%	-69%
15	-249%	-294%	-675%	-23%	52%	23%	-7%	-26%	-42%	-52%
	=	Morphing bending location at 90% of chord location								
	=	Morphing bending location at 80% of chord location								
	=	Morphing bending location at 70% of chord location								
	=	Morphing bending location at 60% of chord location								
	=	Morphing bending location at 50% of chord location								
X%	=	Showing positive or increased C_L/C_D by X%								

Table 18 Percentage difference of C_D for NACA 2415 trailing edge morphing bending angle compared to 90% chord location at 0°

Trailing edge morphing location/type of data compared with (%)	Data compared with	Morphing bending angle						
		- 25 (%)	- 15 (%)	- 5 (%)	5 (%)	15 (%)	25 (%)	35 (%)
90	(Compared with CFD reference ata)	145	46	24	24	46	95	154
80	90% chord location	21	53	56	55	52	35	37
70	90% chord location	38	88	97	95	84	53	61
60	90% chord location	82	112	128	127	112	70	78
50	90% chord location	55	125	153	153	129	79	93

Table 19 Optimal wing configuration of NACA 0012 trailing edge morphing for Climbing flight phase

AOA	Range of increased C_L/C_D /%	Morphing location/% of chord location (%)	No of designs	Bending angles/ angle range showing optimal performance	Wing design of maximum performance for a specific AOA
2.5	24–71	90	5	5° till 45°	Figure 29
	2–70	80	3	5° till 25°	
	56 and 42	70	2	5° and 15°	
	27 and 67	60	2	5° and 15°	
	65 and 3	50	2	5° and 15°	
5	9	90	1	15°	Figure 30
	4	80	1	5°	
	5	70	1	5°	
	5	60	1	5°	
	3	50	1	5°	
10	10–134	90	8	– 45° till 25°	Figure 31
	31–144	80	4	– 15° till 15°	
	165 and 106	70	2	– 5° and 5	
	170 and 55	60	2	– 5° and 5	
	180 and 67	50	2	– 5° and 5	
12.5	53, 11,23 and 16	90	4	– 25°, – 5°, 15° and 25°	Figure 32
	53	80	1	– 15° and – 5°	
	30	70	1	5°	
	59	60	1	– 5°	
	138 and 4	50	2	– 5° and 5°	
15	1–60	90	10	– 45° till 45°	Figure 33
	8–48	80	5	– 45°, – 15 till 15°	
	5–62	70	4	– 15° and – 5°	
	47, 271 and 2	60	3	– 5°, 5 and 15°	
	52 and 23	50	2	– 5° and 5°	

Table 20 Optimal wing configuration of NACA 0012 trailing edge morphing for take-off flight phase

AOA	Percentage of drag reduction	Percentage of increased C_L/C_D	Morphing location/% of chord location	Bending angles showing optimal performance	Number of wing designs	Wing design reference of optimal performance for a specific AOA
10	- 62%	42%	90	- 45	7	Figure 29
	- 70%	62%	90	- 35		
	- 68%	74%	90	- 25		
	- 70%	105%	90	- 15		
	- 54%	86%	90	- 5		
	- 45%	134%	90	5		
	- 31%	80%	90	15		
	- 76%	54%	80	- 15°	3	
	- 63%	144%	80	- 5°		
	- 43%	107%	80	5°		
	- 68%	165%	70	- 5°	2	
	- 40%	106%	70	5°		
	- 71%	170%	60	- 5°	2	
	- 19%	55%	60	5°		
	- 73%	180%	50	- 5°	2	
- 26%	67%	50	5°			
12.5	- 45%	53%	90	- 25°	2	Figure 31
	- 22%	11%	90	- 5°		
	- 56%	53%	80	- 15°	2	
	- 27%	53%	80	- 5°		
	- 20%	59%	60	- 5°	1	
	- 48%	138%	50	- 5°	1	
15	- 25	3	90	- 45°	4	Figure 33
	- 45	13	90	- 35°		
	- 51	60	90	- 25°		
	- 49	33	90	- 15°		
	- 42	48	80	- 15°	3	
	- 48	8	80	45°		
	- 9	38	80	5°		
	- 64	16	70	- 15°	3	
	- 2	62	70	- 5°		
	- 5	31	70	5°		
	- 61	47	60	- 15°	2	
	- 2	27	60	5°		
- 29	52	50	- 5°	1		

Table 21 Findings and comparisons of trailing edge morphing for NACA 2415 and NACA 0012

Flight phase	Total number of optimal wing configuration/preferred designs	Wing design Reference of NACA 2415 for optimal performance	Wing design Reference of NACA 0012 for optimal performance	Findings
Cruise	NACA 2415: 3 NACA 0012: 0	Figure 18	None	At zero AOA, NACA 2415 showed 3 potential wing configurations showed drag reduction, while NACA 0012 showed no improvement for the cruise flight phase. Asymmetric airfoil has a better impact when the trailing edge morphing concept applied for the cruise flight phase
Climbing flight phase	NACA 2415: 77 NACA 0012: 70	Figure 19	Figure 29	Both symmetric and asymmetric airfoils showed significant improvement in the climbing flight phase
Take-off flight phases	NACA 2415:30 NACA 0012:35	Figure 23	Figure 31	Both symmetric and asymmetric airfoils showed significant improvement in the take-off flight phase
descending and landing flight phase	bending angle ranging from -5° till -45° , for all morphing bending location	Figure 25	Figure 32	Both symmetric and asymmetric airfoils showed significant improvement for the descending and landing flight phase

Acknowledgements The Computing and library resources are provided by Taylor's University, School of Engineering.

Author Contributions Design of work and conceptualization by AK and ASMA. All research analysis and other work conducted by AK.. Review of research work by AK and ASMA. Under Supervision of ASMA and Co-supervised by FWYM. Manuscript drafted by AK. Manuscript review and edited by AK and ASMA. All authors read and approved the final manuscript.

Funding There is no funding to support this research.

Availability of Data and Materials All data generated or analyzed during this study are included in this published article with appropriated citations.

Declarations

Conflict of interest The authors confirm that they have no competing interest.

References

- Concilio A, Lecce L (2018) Historical background and current scenario. Morphing wing technologies: large commercial aircraft and civil helicopters. Elsevier Inc, Oxford, pp 3–84. <https://doi.org/10.1016/B978-0-08-100964-2.00001-0>
- Bowman J, Sanders B, Weisshaar T (2002) Evaluating the impact of morphing technologies on aircraft performance. In: 43rd AIAA/ASME/ASCE/AHS/ASC structures, structural dynamics, and materials conference. American Institute of Aeronautics and Astronautics. <https://doi.org/10.2514/6.2002-1631>
- Savastano E, Perez-Sanchez V, Arrue BC, Ollero A (2022) High-performance morphing wing for large-scale bio-inspired unmanned aerial vehicles. *IEEE Robot Automat Lett* 7(3):8076–8083. <https://doi.org/10.1109/LRA.2022.3185389>
- Ameduri S, Concilio A (2020) Morphing wings review: aims, challenges, and current open issues of a technology. *Proc Inst Mech Eng Part C J Mech Eng Sci*. <https://doi.org/10.1177/0954406220944423>
- Sofla AYN, Meguid SA, Tan KT, Yeo WK (2010) Shape morphing of aircraft wing: status and challenges. *Mater Des* 31(3):1284–1292. <https://doi.org/10.1016/j.matdes.2009.09.011>
- La S, Joe WY, Akbar M, Alsaïdi B (2018) Surveys on skin design for morphing wing aircraft: status and challenges. In: 2018 AIAA

- aerospace sciences meeting. American Institute of Aeronautics and Astronautics. <https://doi.org/10.2514/6.2018-0315>
7. Chandler D (2019) MIT and NASA engineers demonstrate a new kind of airplane wing. Massachusetts Institute of Technology News. <https://phys.org/news/2019-04-mit-nasa-kind-airplane-wing.html>
 8. Franke J, Hirsch C, Jensen G, Krüs HW, Miles S, Schatzmann M, Westbury PS, Wisse JA, Wright NG (2004) Recommendations on the use of CFD in wind engineering
 9. Argyropoulos CD, Markatos NC (2015) Recent advances on the numerical modelling of turbulent flows. *Appl Math Model* 39(2):693–732. <https://doi.org/10.1016/j.apm.2014.07.001>
 10. Bendjebbas H, Abdellah-ElHadj A, Abbas M (2016) Full-scale, wind tunnel and CFD analysis methods of wind loads on heliostats: a review. *Renew Sustain Energy Rev* 54:452–472
 11. Singh J, Singh J, Singh A, Rana A, Dahiya A (2015) Study of NACA 4412 and Selig 1223 airfoils through computational fluid dynamics. *Int J Mech Eng* 2(6):17–21. <https://doi.org/10.14445/23488360/ijme-v2i6p104>
 12. Salazar-Jiménez G, López-Aguilar H, Gómez JA, Chazaro-Zaharias A, Duarte-Moller A, Pérez-Hernández A (2018). Blended wing' CFD analysis: aerodynamic coefficients
 13. Yokozeki T, Sugiura A, Hirano Y (2014) Development of variable camber morphing airfoil using corrugated structure. *J Aircr* 51(3):1023–1029. <https://doi.org/10.2514/1.C032573>
 14. Ouyang Y, Gu Y, Kou X, Yang Z (2021) Active flutter suppression of wing with morphing flap. *Aerosp Sci Technol* 110:106457. <https://doi.org/10.1016/j.ast.2020.106457>
 15. Chaviaropoulos PK (1999) Flap/lead-lag aeroelastic stability of wind turbine blade sections. *Wind Energy* 2(2):99–112. [https://doi.org/10.1002/\(sici\)1099-1824\(199904/06\)2:2%3c99::aid-we21%3e3.0.co;2-u](https://doi.org/10.1002/(sici)1099-1824(199904/06)2:2%3c99::aid-we21%3e3.0.co;2-u)
 16. Chaviaropoulos PK, Soerensen NN, Hansen MOL, Nikolaou IG, Aggelis KA, Johansen J, Gaunaa M, Hambraus T, Von Geyr H, Hirsch C, Shun K, Voutsinas SG, Tzabiras G, Perivolaris Y, Dyrmoose SZ (2003) Viscous and aeroelastic effects on wind turbine blades. The VISCEL project. Part II: aeroelastic stability investigations. *Wind Energy* 6(4):387–403. <https://doi.org/10.1002/we.101>
 17. Shortal JA, Maggin B (1946) Effect of sweepback and aspect ratio on longitudinal stability characteristics of wings at low speeds. In: Naca-Tp-1093. National Advisory Committee for Aeronautics
 18. Rauleder J, Van Der Wall BG, Abdelmoula A, Komp D, Kumar S, Ondra V, Titurus B, Woods BKS (2018) Aerodynamic performance of morphing blades and rotor systems. Annual forum proceedings—AHS international, 2018-May, 12708. <https://research-information.bris.ac.uk/en/publications/aerodynamic-performance-of-morphing-blades-and-rotor-systems>
 19. Akhter MZ, Ali AR, Omar FK (2022) Effect of flow Reynolds number on the aerodynamics of a novel bionic morphing flap. In: 2022 Advances in science and engineering technology international conferences (ASET), pp 1–6. <https://doi.org/10.1109/ASET53988.2022.9734807>
 20. Zhang Y, Ge W, Zhang Z, Mo X, Zhang Y (2019) Design of compliant mechanism-based variable camber morphing wing with nonlinear large deformation. *Int J Adv Rob Syst* 16(6):1729881419886740. <https://doi.org/10.1177/1729881419886740>
 21. Wang L, Zuo X, Liu H, Yue T, Jia X, You J (2019) Flying qualities evaluation criteria design for scaled-model aircraft based on similarity theory. *Aerosp Sci Technol* 90:209–221. <https://doi.org/10.1016/j.ast.2019.04.032>
 22. Banazadeh A, Hajipouzadeh P (2019) Using approximate similitude to design dynamic similar models. *Aerosp Sci Technol* 94:105375. <https://doi.org/10.1016/j.ast.2019.105375>
 23. Selig MS, Guglielmo JJ, Broeren AP, Giguère P (1995) Summary of low speed airfoil Dara—vol 1. In: Uicc, vol 1. SoarTech Publ.
 24. Kabir A, Al-Obaidi ASM, Myan FWY (2023) Review and aerodynamic analysis of NACA 2415 morphing wing for variable span and scale morphing concepts using CFD analysis. *J Phys Conf Ser* 2523(1):012033. <https://doi.org/10.1088/1742-6596/2523/1/012033>
 25. Cantwell BJ (2014) Chapter 12 Wings of Finite Span. In: Applied aerodynamics (Issue c, pp. 1–62). <https://web.stanford.edu/~cantwell/#c6> PP—Stanford University. https://web.stanford.edu/~cantwell/AA200_Course_Material/AA200_Course_Notes/AA200_Ch_12_Wings_of_Finite_Span_Cantwell.pdf
 26. Anderson JD (2017) Chapter 5: incompressible flow over finite wings. In: Anderson JD (ed) Fundamentals of aerodynamics, 6th edn. McGraw-Hill Education, New York, pp 427–432
 27. Sadraey MH (2012) Wing design. In: Aircraft design, pp 161–264. <https://doi.org/10.1002/9781118352700.ch5>
 28. Zhu Y, Wang J, Chen Y, Wu Y (2016) Calculation of takeoff and landing performance under different environments. *Int J Mod Phys Conf Ser* 42:1660174. <https://doi.org/10.1142/s2010194516601745>
 29. Zhang M, Huang Q, Liu S, Zhang Y (2019) Fuel consumption model of the climbing phase of departure aircraft based on flight data analysis. In: Sustainability (Switzerland), vol 11, Issue 16. <https://doi.org/10.3390/su11164362>
 30. Poll DIA, Schumann U (2021) An estimation method for the fuel burn and other performance characteristics of civil transport aircraft in the cruise. Part I fundamental quantities and governing relations for a general atmosphere. *Aeronaut J* 125(1284):257–295. <https://doi.org/10.1017/aer.2020.62>
 31. Poll DIA, Schumann U (2021) An estimation method for the fuel burn and other performance characteristics of civil transport aircraft during cruise: part 2, determining the aircraft's characteristic parameters. *Aeronaut J* 125(1284):296–340. <https://doi.org/10.1017/aer.2020.124>
 32. Murrieta-Mendoza A, Botez RM (2015) Methodology for vertical-navigation flight-trajectory cost calculation using a performance database. *J Aerosp Inf Syst* 12(8):519–532. <https://doi.org/10.2514/1.I010347>
 33. Raymer D (2019) Aircraft design: a conceptual approach, Sixth Edition and RDSwin Student SET. In: Aircraft design: a conceptual approach, sixth edition and RDSwin student SET. <https://doi.org/10.2514/4.105746>

Publisher's Note Springer Nature remains neutral with regard to jurisdictional claims in published maps and institutional affiliations.

Springer Nature or its licensor (e.g. a society or other partner) holds exclusive rights to this article under a publishing agreement with the author(s) or other rightsholder(s); author self-archiving of the accepted manuscript version of this article is solely governed by the terms of such publishing agreement and applicable law.